Polymorph engineering of TiO_2: demonstrating how absolute reference potentials are determined by local coordination

John Buckeridge,[*,†] Keith T. Butler,[‡] C. Richard A. Catlow,[†] Andrew J. Logsdail,[†] David O. Scanlon,[†,¶] Stephen A. Shevlin,[†] Scott M. Woodley,[†] Alexey A. Sokol,[†] and Aron Walsh[‡]

†University College London, Kathleen Lonsdale Materials Chemistry, Department of Chemistry, 20 Gordon Street, London WC1H 0AJ, UK

‡Centre for Sustainable Chemical Technologies and Department of Chemistry, University of Bath, Claverton Down, Bath BA2 7AY, UK

¶Diamond Light Source Ltd., Diamond House, Harwell Science and Innovation Campus, Didcot, Oxfordshire OX11 0DE, United Kingdom

E-mail: j.buckeridge@ucl.ac.uk

Abstract

We report that the valence and conduction band energies of TiO_2 can be tuned over a 4 eV range by varying the local coordination environments of Ti and O. We examine the electronic structure of eight known polymorphs and align their ionization potential and electron affinity relative to an absolute energy reference, using an accurate multi-scale quantum-chemical approach. For applications in photocatalysis, we identify the optimal combination of phases to enhance activity in the visible spectrum. The results provide a coherent explanation for a wide range of phenomena, including the performance of TiO_2 as an anode material for Li-ion batteries, allow us to pinpoint hollandite TiO_2 as a new candidate transparent conducting oxide, and serve as a guide to improving the efficiency of photoelectrochemical water splitting through polymorph engineering of TiO_2.

Introduction

Optical and electronic engineering of metal oxides for a range of technological applications has led to the study of increasingly complex multi-component systems, recently including mixed-anion solid solutions for modification of the valence band energy.[1–7] The inherent chemical and structural disorder of multi-component systems results in variation in materials properties and performance, and provides a major challenge for scaling up towards application on a commercial scale. An alternative approach is to start with fewer chemical components and control the *structure* rather than the *composition*, which is the topic addressed in this study.

Most metal oxides can adopt a range of crystal structures depending on the preparation and treatment conditions. In addition to known polymorphs in the equilibrium phase diagram, the development of non-equilibrium growth techniques, such as atomic-layer deposition, provides an opportunity to exploit hitherto unknown metastable structural configurations.[8]

The importance of local structure in determining the observable properties of a material has been discussed since the advent of crystallography.[9] In the context of ionic solids, a key descriptor is the Madelung potential of each crystallographic site, which is determined by a summation to infinity over the ionic charges of the surrounding ions.[10] Knowledge of the variations in the local electrostatic potential proved key to the development of theories of work functions,[11] defect chemistry including ionic conductivity,[12] and even, for example, to the understanding of the nature of hole pairing in high-temperature superconductors.[13]

Since the discovery in 1972 by Fujishima and Honda[14] of the ability of TiO_2 to split water using sunlight, there has been extensive research into improving the efficiency of this process. It has been found that samples containing a mixture of the most abundant phases of TiO_2, anatase and rutile, outperform pure phase samples.[15] We have recently explained this behaviour by the variation in the electrostatic potential of Ti and O in the two polymorphs, which drives changes in the ionisation potential and electron affinity (work function) of the materials.[16] The idea of mixing other known polymorphs of TiO_2, including brookite and TiO_2-B, is a natural extension of this concept, but has to date not been explored.

A key requirement for the water splitting process is that the electronic energy bands of the photoelectrode are aligned with respect to the redox potentials of water. In electronic structure calculations, under periodic boundary conditions, there is no absolute reference potential.[17] The absence of a well-defined vacuum level hinders prediction of the suitability of novel materials for photoelectrochemical, or indeed photovoltaic or other optoelectronic, applications. To overcome this problem, we have developed a multi-region, quantum mechanical / molecular mechanical (QM/MM) solid-state embedding procedure. The embedding procedure exploits the 'tin-foil' boundary condition in the three-dimensional electrostatic (Ewald) summation to provide an absolute reference. This approach advantageously treats all possible charge (oxidation) states of the defect (e.g. created by electron addition or removal) within the same reference frame.

In this work, we consider all four naturally occurring TiO_2 phases, as well as four phases

that have been sythesised experimentally. We relate the variations in ionisation potential and electron affinity of each polymorph to the differences in crystal structure, and in particular to the local coordination environments and medium-range order of oxygen and titanium. To complement our embedding procedure, density functional theory (DFT) within periodic boundary conditions is used to calculate the full electronic band structure of each material, and to construct a complete band alignment scheme for the binary TiO_2 system. The scheme developed here should provide a solid foundation for future studies and optimisation of titania based materials and devices, but has a relevance to a wider range of metal oxide applications.

Computational details

We utilise two approaches to determine the electronic energy bands of each polymorph of TiO_2 relative to vacuum.

Solid-state Embedding

We employ a hybrid QM/MM embedded cluster approach, as implemented in the `ChemShell` code,[64,65] which provides direct access to the vacuum level without any surface present. The method for calculating I consists of modelling a charged defect (in this case a hole at the top of the valence band in bulk) within a cluster of about 80 atoms treated at a QM level of theory, which is embedded in a larger cluster of about 10,000 atoms treated at a MM level of theory. The MM cluster is modelled using a polarisable shell interatomic forcefield[66] that accurately reproduces the high-frequency dielectric tensor of bulk,[12,16] so that it provides the correct polarisation response of the surrounding infinite solid to the charged defect in the QM region. In this way the defect is treated at the dilute limit.[67]

I is determined using a ΔSCF (self-consistent field) approach, i.e. by calculating the energy difference between the system in the neutral and positive charge states. The accuracy of this approach is well established.[16,52,68–72]

Cluster Size

For each phase, a spherical cut of the bulk material of radius 30 Å was taken. This sphere was then surrounded by point charges, the charge of which were fitted to reproduce the Madelung potential of the infinite system within the central region of the sphere (with a tolerance of 10^{-6} V). The sphere is then divided into a QM region at the centre, surrounded by an interface region, then an active MM region, then a 15 Å wide frozen MM region (see Ref.[67] for more details). The QM region need not be stoichiometric nor charge neutral owing to the boundary conditions of the cluster model. We used different QM region sizes in order to test for convergence. For rutile, anatase, brookite, TiO_2-B, α-PbO_2, baddeleyite, hollandite, and ramsdellite the smaller QM cluster size consisted of 55, 47, 51, 47, 69, 91, 43, 43 atoms, respectively; the larger QM cluster size consisted of 71, 79, 71, 93, 89, 102, 73, 79 atoms, respectively. The resulting ionisation potentials were converged within approximately 2%.

QM Region

QM calculations were done using the `Gamess-UK`[73] code. A triple-zeta valence plus polarisation Gaussian basis set was used for Ti and O ions, with a 10 core electron effective core potential (ECP) used in modelling Ti atoms.[74,75] Electron exchange and correlation were treated at the level of hybrid meta-GGA, as parametrised in the BB1k formalism,[76] which gives a highly accurate description of electron localisation, atomisation energies and thermochemistry.

MM Region

MM calculations were performed using the `GULP` code.[77] The shell polarisable interatomic forcefield we have used to treat the MM region is a modification of a forcefield model previously derived to treat $SrTiO_3$,[12,16] which was based on the Born model of ionic solids.[78] The model is designed to reproduce the high frequency dielectric properties of TiO_2, meaning

that it has been employed to relax electronic degrees of freedom only. We simulate ion-ion interactions as two-body interactions using a Coulomb sum:

$$U_{ij}^{Coulomb} = \frac{q_i q_j}{r_{ij}},\tag{1}$$

where U_{ij} is the energy of interaction and r_{ij} is the separation between ions i and j, and q_i is the charge on ion i; and using a Buckingham potential, including a dispersion term, of the form

$$U_{ij}^{Buck} = A \exp(r_{ij}/\rho) - \frac{C}{r_{ij}^6},\tag{2}$$

where the parameters A, ρ, and C depend on species i and j.

The polarizability of the ions is taken into account using the shell model of Dick and Overhauser,[66] where each ion is separated into a core and shell, with the massless shell (charge Y) connected to the core by a spring. The total charge of the core-shell equals the formal charge of the ion. The energy is given by:

$$U_{c-s} = \frac{1}{2} K r_{c-s}^2 + \frac{1}{24} K_4 r_{c-s}^4,\tag{3}$$

where K and K_4 are the spring constants and r_{c-s} is the distance between the core and shell. The parameters used are given in Table 1. This force field model was also used in calculating the Madelung potentials and defect energies within the Mott-Littleton[11] approach. We note that, in using a common reference, i.e. the vacuum level, we are able to compare directly calculated ionisation potentials across the different polymorphs.

Interface Region

To treat the interface between the QM and MM regions, a specially designed local effective core pseudopotential (ECP) was placed on Ti sites located within a range of 5 Å from the

Table 1: Interatomic potential parameters for bulk TiO_2, including shell polarization on Ti and O ions (e is the electron charge).

Buckingham	A (eV)	ρ (Å)	C (eVÅ^{-6})
O shell — O shell	22764.3	0.15	43.0
O shell — Ti shell	835.0	0.38	9.6
Shell	K (eVÅ^{-2})	$Y(e)$	K_4 (eVÅ^{-4})
Ti core — Ti shell	981.4	-1.00	50000
O core — O shell	11.7	-2.39	50000

edge of the QM region.[16] The ECP $U_p(r)$ has the form:

$$r^2 U_p(r) = A_1 r \exp(-Z_1 r^2), \tag{4}$$

where the parameters A_1 and Z_1 were fitted in order to minimize the gradients on the ions in the QM and interface region, and the spread of deep core levels in the energy spectrum. The parameters are (in atomic units) $A_1 = 0.935$, $Z_1 = 0.356$.

Periodic Models of the Ideal Solid

The band gap of each polymorph was determined using plane-wave DFT, treating electron exchange and correlation with the screened hybrid HSE06 functional.[79] We use plane-wave DFT, as calculating the electron affinity accurately would require a bigger cluster model and basis sets that are much too large for current computing resources. When calculating I using the ΔSCF approach, the BB1k functional accounts for the self-interaction error,[16] while when calculating E_g the HSE06 functional describes well the periodic solid, and indeed is known to reproduce accurately the band gaps of rutile and anatase.[61]

The plane-wave DFT calculations were performed using the VASP code,[80–83] with the projector augmented wave approach[84] used to describe the interaction between the core (Ti:[Ar], O:[He]) and valence electrons. A plane-wave cut-off of 500 eV was used in each case, and for the rutile, anatase, brookite, TiO_2-B, α-PbO_2, baddeleyite, hollandite, and ramsdellite phases we used a $4 \times 4 \times 6$, $4 \times 4 \times 4$, $2 \times 4 \times 4$, $4 \times 4 \times 4$, $4 \times 4 \times 4$, $4 \times 4 \times 4$,

$3 \times 3 \times 3$, and a $2 \times 6 \times 4$ special k-points mesh centred at the Γ point, respectively. These settings provided total energy convergence within 10^{-4} eV/atom. The band gap calculations were performed using unit cells derived from the experimental lattice parameters, with the ions kept at their experimentally determined positions.

Results and Discussion

Polymorphs of TiO_2

The crystal structures of the eight polymorphs considered here are shown in Figure 1. In all our calculations, we fix the ionic coordinates at the experimentally determined values and relax the electronic degrees of freedom. Performing the calculations in this manner means that a comparison of the total energies of the phases is of limited value; nevertheless the calculated energies are all thermodynamically accessible (at room temperature), which corroborates the structural stability of the polymorphs studied. The naturally occurring phases considered are (space groups in parantheses): rutile $(P4/mnm)$,[18] anatase $(I4_1/amd)$,[19] brookite $(Pbca)$,[20] and TiO_2-B $(C2/m)$.[21] The synthetic polymorphs include the high-pressure phases α-PbO_2 $(Pbcn)$[22] and baddeleyite $(P2_1/c)$[23] (in the limit of ambient pressure) and the nanoporous phases hollandite $(I4/m)$[24] and ramsdellite $(Pbnm)$.[25]

Each polymorph typically consists of ordered arrays of TiO_6 distorted octahedra, with 3-coordinated oxygens, apart from the baddeleyite phase which has 7-coordinated Ti and a mix of 2- and 4-coordinated O, and the TiO_2-B phase which has 2-, 3-, and 4-coordinated O. The phases differ in the order, distortion, and connectivity of the polyhedra.[26,28] Relevant structural data can be gleaned from publicly accessible databases, $e.g.$, see Ref.[27]

Absolute Electronic Energy Levels

We report the calculated ionisation potential (I), determined using the hybrid QM/MM approach, the energy band gap (E_g), determined using plane-wave DFT, and the derived
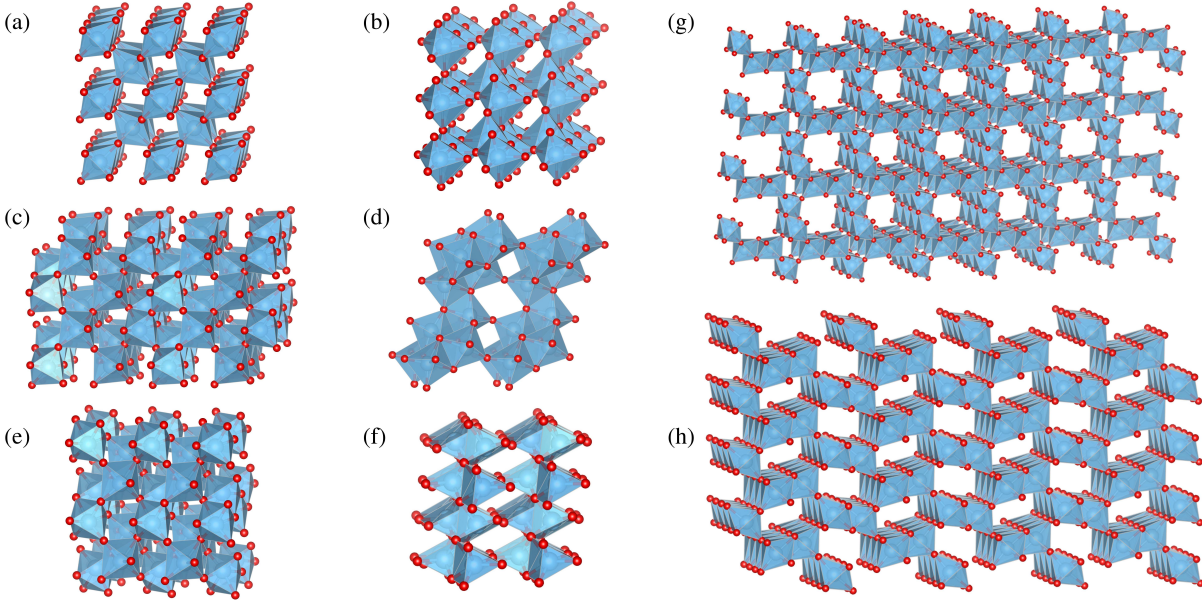
Figure 1: The different phases of TiO$_2$ considered in this study: (a) rutile, (b) anatase, (c) brookite, (d) TiO$_2$-B, (e) α-PbO$_2$, (f) baddeleyite, (g) hollandite, (h) ramsdellite (see text for references and space groups). Polyhedra consisting of Ti atoms and nearest-neighbour O are represented in blue. O atoms are represented by red spheres.

electron affinity (A, where $A = I - E_g$) of each polymorph in Table 2, and depict the resulting band alignment, relative to an absolute vacuum potential in Figure 2. These values are compared to the position of the redox potentials of water obtained from the standard hydrogen electrode potential ($E(\mathrm{H^+/H_2}) = 4.44$ V relative to vacuum at room temperature[29]) and the water-splitting free energy of 1.23 eV.[30–32] For comparison, we show in Table 2 experimentally determined values of E_g where available. For rutile and anatase, the band gap values are from low temperature and ambient pressure measurements,[33,34] while for the less-well studied brookite phase we show the range of experimental values that have been reported.[35]

Variation in the ionisation potential, electron affinity and band gap of 4.39 eV, 2.73 eV and 1.91 eV, respectively, is calculated across the eight polymorphs. The baddeleyite phase exhibits an anomalous behaviour, with an exceptionally high position of the valence band (low ionisation potential of 4.77 eV) and a much lower electron affinity (work function

Table 2: Calculated ionization potential (I), determined using a ΔSCF approach within a QM/MM embedded cluster model, energy band gap (E_g), determined using plane-wave DFT with a hybrid functional, and derived electron affinity ($A = I - E_g$) of each of the TiO_2 polymorphs. Experimental values of E_g are given for comparison where available.

Polymorph	I (eV)	E_g (eV)	A (eV)	Expt. E_g (eV)
Rutile	7.83	3.10	4.73	3.031[a]
Anatase	8.30	3.36	4.94	3.23[b]
Brookite	7.66	3.51	4.15	$3.1 - 3.4$[c]
TiO_2-B	7.97	4.11	3.86	−
α-PbO_2	7.89	3.81	4.08	−
Baddeleyite	4.77	2.20	2.57	−
Hollandite	9.16	3.86	5.30	−
Ramsdellite	8.05	3.78	4.27	−

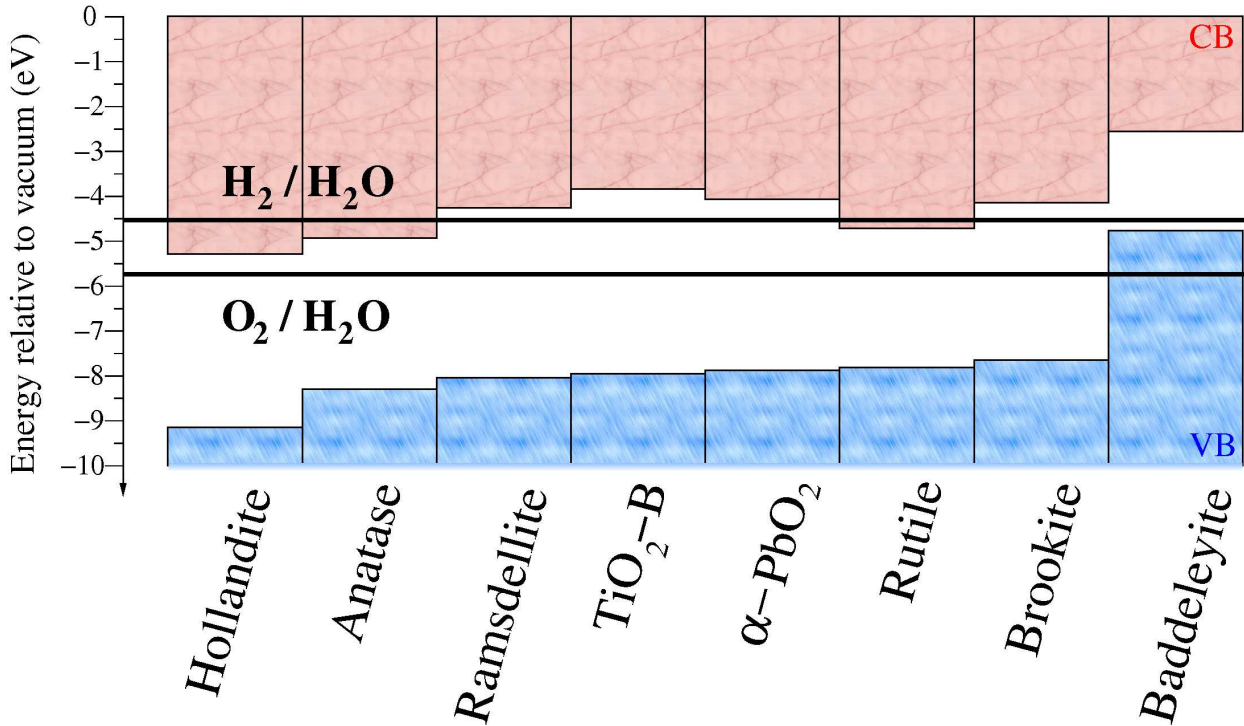[a]Ref.,[33] [b]Ref.,[34] [c]Ref.[35]

Figure 2: Calculated valence band (VB) and conduction band (CB) positions relative to the vacuum level for the various TiO_2 polymorphs considered, shown in comparison with the H_2 and O_2 redox potentials.

of 2.57 eV), which combine to give a significantly reduced band gap of 2.2 eV. From the other phases, the maximum value of I is found for the hollandite phase (9.16 eV), while the

minimum value is obtained for brookite (7.66 eV).

The baddeleyite phase is different from the others in terms of its coordination of Ti (7 as opposed to 6), and has a mix of 2- and 4-coordinated O, which only the TiO_2-B phase shares. The Madelung potential (V_M) at each ionic site has been calculated, taking into account the intrinsic electron polarisation of each polymorph. We find that the two differently coordinated O sites in baddeleyite have quite different values of V_M, 22.5 and 29.9 V for 2- and 4-coordinated, respectively. Lower potentials indicate higher electronic energies at anionic sites. The low Madelung potential at the low coordination site correlates well with the dramatic offset in the values of the ionisation potential between baddeleyite and the other phases. Indeed, on comparing the relevant V_M we find a 3.6 eV offset between baddeleyite and brookite, in agreement with the trend we observe using our QM/MM approach.

To provide further support to the preceding analysis, we employ the approach of Mott and Littleton,[11] which includes dynamic polarisation effects of the extended crystal. Here, the ionisation process is simulated as the formation of a hole on an oxygen site. In TiO_2, the valence band is formed predominately from overlap of oxygen $2p$-like states (see the electronic density of states in Figure 4) as seen universally in other *ab initio* electronic structure calculations[37] and from photoemission spectroscopy.[38] Following the self-consistent Mott-Littleton procedure, which accounts for electronic relaxation in response to hole formation, we calculated the ionisation potentials for the titania polymorphs in close agreement with the *ab initio* QM/MM data. We have obtained in fact an improvement on the results based on the Madelung potentials. Crucially, comparing the quasi-particle hole energy between the brookite and baddeleyite phases (cf. 3.1 eV vs. 2.9 eV from the Mott-Littleton and QM/MM approaches respectively), we observe the same dramatic offset as quantum chemical simulations.

To rationalise the difference in behaviour, we now investigate the local environment of the polymorphs in further detail. In baddeleyite, the titanium coordination can be viewed as trigonal prismatic (6-fold coordinate), where the prisms form an edge-sharing bilayer
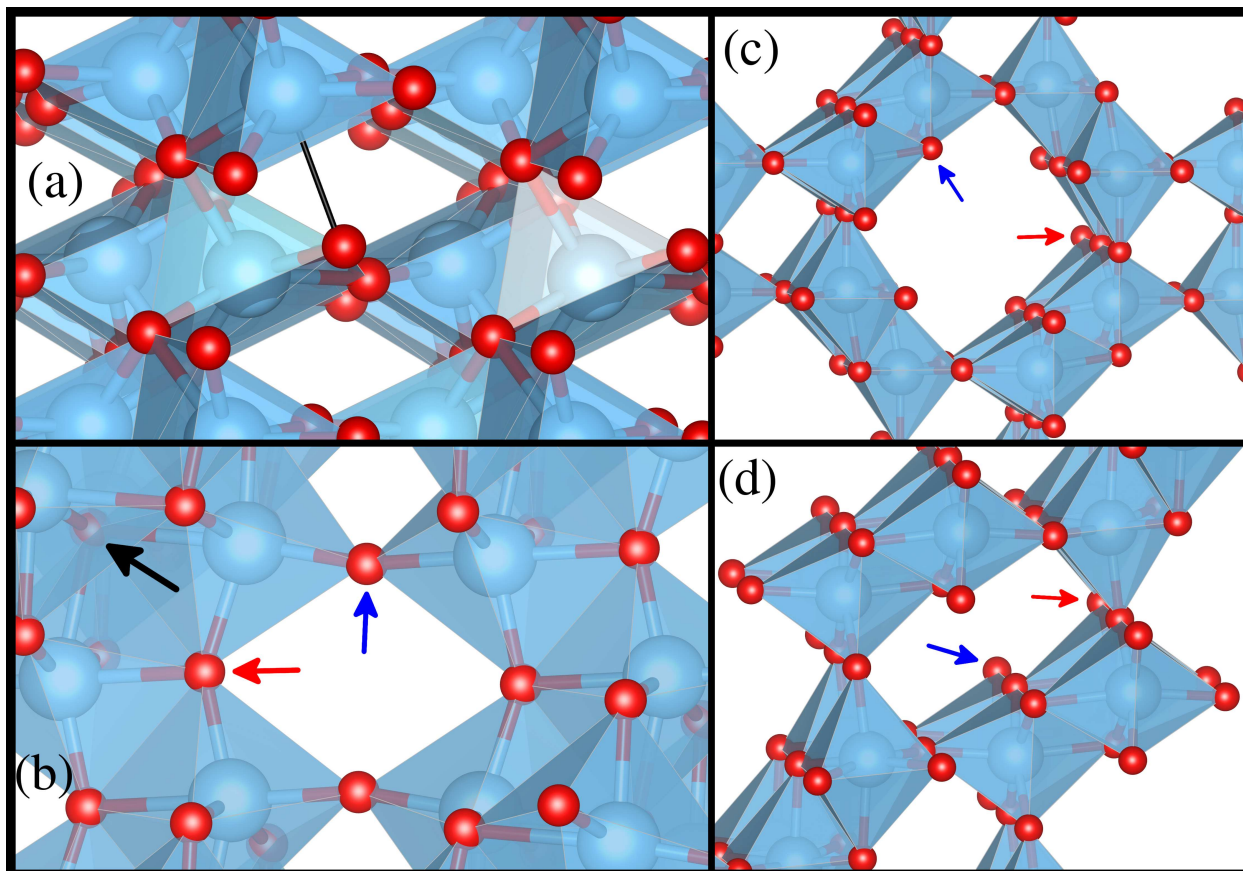
11

Figure 3: A more detailed view of the local structure in (a) the baddeleyite phase, where the bridging bond between a 2-coordinated oxygen and the titanium at the centre of a second-nearest neighbour trigonal prism is shown in black; (b) the TiO_2-B phase, where 2-, 3-, and 4-coordinated oxygens are indicated by blue, red, and black arrows respectively; (c) the hollandite and (d) ramsdellite phases, indicating a trigonal planar coordination site (red arrow) and a trigonal pyramidal coordination site (blue arrow).

network (see Figure 3(a)). Two oxygen ions, defining one of the prism side edges, bridge between adjacent bilayers, and connect two nearest prisms within a layer. At the same time, a third longer coordinate bond is formed between each of these oxygens and a second-nearest neighbour prism (giving rise to the seventh Ti–O bond). This latter oxide stands out in its properties, which are directly correlated to the local atomic structure. Indeed, all other polymorphs of TiO_2 consist of edge and corner sharing octahedra, rather than prisms, and the only other example of a two coordinated oxygen is the linear bridge between adjacent octahedral bilayers found in TiO_2-B.

A similar set of arguments helps explain the behaviour of band edges in the other polymorphs. In the first instance, we consider the hollandite phase, which has the largest I of all the polymorphs. Analysing the local coordination of oxygen ions (see Figure 3(c) and (d)), we observe two basic environments which are shared by both nanoporous phases, ramsdellite and hollandite: in one the ion is surrounded by three Ti sites in a slightly distorted planar trigonal configuration; in the other the oxygen ion has a trigonal pyramidal coordination. The former configuration is common to many TiO_2 polymorphs including the three most common: rutile, anatase and brookite. We find that, in the perfect crystal, the Madelung potential on the trigonal pyramidal site, in comparison with the planar site, is significantly less stable (by 0.9 V). The order, however, is reversed when we use the Mott-Littleton approach (allowing all electronic degrees of freedom to relax), due to the strong stabilisation of the trigonal pyramidal sites by the Madelung field - a local polarisation effect. Furthermore, hollandite has a particularly porous structure, where the Coulomb interaction between oxygen ions across the channels (or pores) is much weaker than in its denser counterpart polymorphs, including even the other nanoporous structure (ramsdellite). This structural motif could be utilised in future polymorph engineering studies aimed at obtaining novel materials with a deep position of the valence band.

For the TiO_2-B phase, which has 2-, 3-, and 4-coordinated oxygen ion sites (see Figure 3(b)), we calculate the least stable V_M at the 2-coordinated sites, with a potential offset of 2.3 V. V_M at the 3- and 4-coordinated sites is in fact similar in value to that in other octahedral polymorphs. From our quantum chemical calculations (see Figure 2), we determine the valence band of this phase to lie close to that of ramsdellite, α-PbO_2, and rutile, in contrast to our molecular mechanical result (which would place its valence band ~ 2 eV higher). The origin of this discrepancy lies in the over-estimation of the polarisability of the 2-coordinated sites in this material. Using the Mott-Littleton approach to treat the polarisation more accurately, while appropriately constraining the electron density on the 2-coordinated sites and accounting for differences in the short-range ion-ion interaction, re-

stores the generally very good correlation between the quantum mechanical and molecular mechanical methods, with the discrepancy reducing to ~ 0.1 eV.
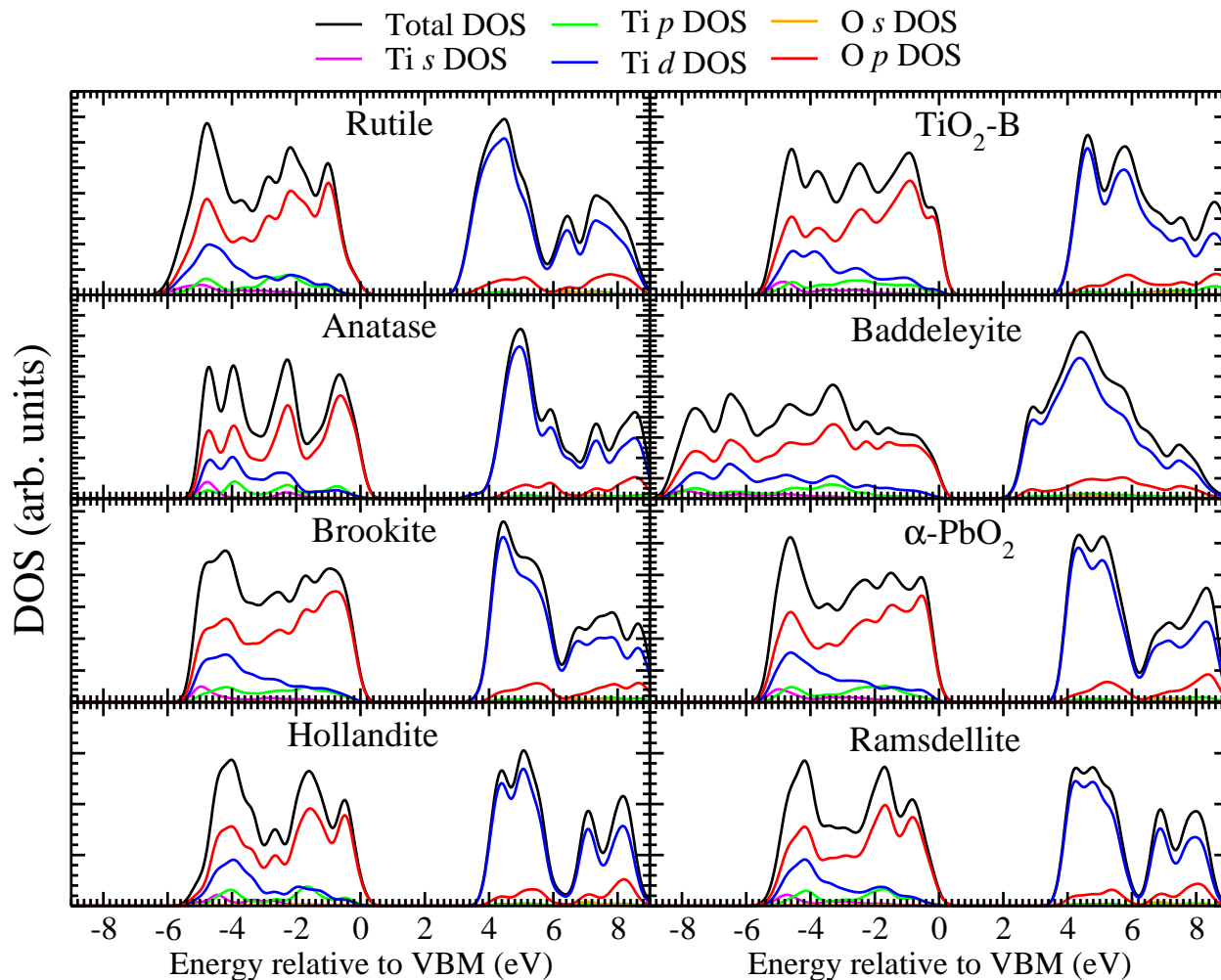

Figure 4: Calculated electronic density of states (DOS) and partial DOS (including contributions from s, p, and d orbitals) of the TiO$_2$ polymorphs as a function of energy relative to the valence band maximum (VBM).

Applications

Photoelectrochemical Water Splitting

The type-II band alignment predicted for the rutile-anatase mixture has two advantages for efficient water-splitting using visible light. Firstly, on excitation, it is favorable for electrons

14

to flow from rutile to anatase, as the CBM of anatase is below that of rutile, and for holes to flow in the opposite direction due to the relative position of the VBMs, which leads to efficient electron–hole separation. Secondly, the effective band gap of the mixture is lower than that of the constituent polymorphs, leading to improved visible light absorption. In water-splitting applications, the most efficient use of available light sources is sought, which is solar radiation in the visible range, hence the desire for materials absorbing in this range. We note that UV sources can also be used in industrial or laboratory settings where high conversion rates can be achieved.

In a recent experiment,[39] it was found that using the α-PbO$_2$ polymorph resulted in an improvement in H$_2$ production from water over using rutile or anatase. We can now explain this observation by comparing the electron affinity of the three phases. We find that the conduction band of the α-PbO$_2$ phase lies 0.37 eV above the reduction potential of water, in contrast to rutile and anatase, where the bulk level is *below* the redox potential. We note that, when the CBM lies below the H$^+$/H$_2$ redox potential, it seems that water splitting will not occur under zero bias; instead a voltage would need to be applied. However, by careful engineering of suitable surfaces or interfaces one can achieve a further offset of the CBM which raises it above the redox potential.

A favourable conduction band position is also found in the brookite phase. Indeed, it has been found experimentally that thin-film samples of brookite TiO$_2$ outperform anatase and rutile.[35,40] We note that the improvement in Ref.[40] was attributed to increased absorption in the visible spectrum due to the presence of defects, which may also play a role in improving performance, but the more favourable band alignment will provide a greater thermodynamic driving force for the reduction reaction.

It is worth also commenting that using baddeleyite, given the calculated valence band position of relative to the water oxidation potential, it should be possible to dampen the H$_2$O oxidation reaction, which could lower the rate of hydroxyl radical formation.

Two factors in the band alignment of rutile and anatase contribute to the enhanced per-

formance of the mixture: increased efficiency of electron-hole separation and a reduction in the effective band gap. From Figure 2 we can conclude that an enhancement of both of these factors should be possible by mixing anatase with either the brookite, TiO_2-B, or α-PbO_2 polymporphs. We therefore predict that improved performance can be achieved using mixtures of anatase with these three polymorphs. To our knowledge, water splitting using such mixtures has not yet been attempted. We note, however, that anatase/TiO_2-B mixed samples have been used for photocatalytic sulfurhodamine-B degradation,[41] and anatase/brookite mixed samples have been used for photocatalytic methylene blue degradation.[42] In both cases, it was found that the mixed phase samples outperformed the pure phases, which would follow from our calculated band alignment and supports our prediction of improved water splitting performance.

Furthermore, a recent study[43] found that mixed anatase/brookite samples showed reduced photoluminescence in comparison to the pure phases, indicating increased charge separation. Again, this result would follow from our calculated band alignment.

While producing mixed phase samples may pose synthetic challenges, a recent procedure reported in Ref.[44] may be ideal for testing our predictions. The approach has been used to form epitaxially sharp anatase/TiO_2-B interfaces, with a minimum of stacking faults or dislocation defects, but could also be applied to the other polymorphs discussed here. Ref.[44] also provided the results from DFT calculations, which confirmed the spatially separated valence and conduction band edges by analysing the electron density. They found that the valence states were localised in the TiO_2-B layer and the conduction states in the anatase layer. Their results, obtained using a different electronic structure approach, agree well with our calculated TiO_2-B/anatase band alignment.

Electrochemical Energy Storage

Our calculated electronic band alignment reveals an important factor that contributes to TiO_2-B outperforming both anatase and rutile as an anode for lithium-ion batteries.[45]

16

The conduction band position of TiO_2-B is closer to the vacuum level than that of both anatase and rutile. The electronic chemical potential of TiO_2-B is higher than that of the other two phases, therefore its open-cell voltage is also higher. Importantly, its electrochemical potential remains below the redox potential of common liquid electrolytes.[46,47] The open-cell voltages for batteries using TiO_2-B, anatase, and rutile are 1.6 V,[45] 1.55 V,[48] and 1.4 V,[49] respectively. If the baddeleyite phase could be stabilised in a form suitable for a battery anode, it could provide a step change in performance.

Optoelectronics

The calculated electron affinity of hollandite is greater than that of all the other polymorphs. Following the doping limit rules, materials with a greater electron affinity are more easily n-type doped.[50–52]

Anatase TiO_2 is an effective transparent conducting oxide (TCO) when donor doped with Nb or F.[53,54] The higher work function of hollandite, together with its large fundamental band gap of 3.86 eV, indicate that it will be a superior *n*-type TCO than anatase, and could be ideal for both conventional *and* ultraviolet TCO applications. The latter is of particular interest for improving the performance of photovoltaic devices as well as short-wavelength light-emitting diodes.[55]

Beyond Bulk Energy Levels

A close look at the literature, including photoemission, electrochemical and thermionic measurements, will reveal a great range in the reported values of work function, ionisation potential and electron affinity of TiO_2.[56] To consider this variation, one must take into account factors that are overlooked by bulk band alignments alone.

Surface termination and morphology,[57–59] as well as features such as charge carrier lifetimes, polaronic trapping, and charge migration to the surface play an important role in photocatalysis and photoelectrochemistry.[15,60–63] These effects should be taken into consid-

eration when explaining the observable properties of all TiO_2 polymorphs.

Despite these factors, bulk band alignment will provide the fundamental energetics upon which a theory of electron and hole dynamics can be built, and constitutes an important initial approximation.

Conclusions

We have calculated the conduction and valence band edge energies relative to vacuum for eight different polymorphs of TiO_2, using a multiscale approach. From our results we determined the titania bulk electronic band alignment, which has been rationalised as an effect of local coordination. The electronic energy levels of each phase are evidently correlated with the Madelung potentials of the constituent ions.

The proposed scheme has been employed to shed light on a number of key technological applications of this class of material. By comparing the band positions on an absolute energy scale, we can explain observed improvements in water splitting performance by the α-PbO_2 and brookite phases and by mixed phase samples. We also give an explanation for the improved performance of TiO_2-B as an anode in Li-ion batteries, and suggest that hollandite TiO_2 should be a superior transparent conducting oxide. Our results serve as a general guide to engineering local structure in order to maximise function in the solid state.

Acknowledgement

References

(1) Maeda, K.; Domen, K. Photocatalytic water splitting: recent progress and future challenges. *J. Phys. Chem. Lett.* **2010**, *1*, 2655–2661.

(2) Chen, S.; Gong, X. G.; Walsh, A.; Wei, S.-H. Crystal and electronic band structure of Cu_2ZnSnX_4 (X = S and Se) photovoltaic absorbers: First-principles insights. *Appl. Phys. Lett.* **2009**, *94*, 041903.

(3) Hiramatsu, H.; Kamiya, T.; Tohei, T.; Ikenaga, E.; Mizoguchi, T.; Ikuhara, Y.; Kobayashi, K.; Hosono, H. Origins of Hole Doping and Relevant Optoelectronic Properties of Wide Gap *p*-Type Semiconductor, LaCuOSe. *J. Am. Chem. Soc.* **2010**, *132*, 15060–15067.

(4) Zakutayev, A.; Tate, J.; Platt, H. A. S.; Keszler, D. A.; Hein, C.; Mayer, T.; Klein, A.; Jaegermann, W. Electronic properties of BaCuChF (Ch = S,Se,Te) surfaces and Ba-CuSeF/ZnPc interfaces. *J. Appl. Phys.* **2010**, *107*, 103713.

(5) Green, D. C.; Glatzel, S.; Collins, A. M.; Patil, A. J.; Hall, S. R. A New General Synthetic Strategy for Phase-Pure Complex Functional Materials. *Adv. Mater.* **2012**, *24*, 5767–5772.

(6) Buckeridge, J.; Scanlon, D. O.; Walsh, A.; Catlow, C. R. A. Automated procedure to determine the thermodynamic stability of a material and the range of chemical potentials necessary for its formation relative to competing phases and compounds. *Comput. Phys. Commun.* **2014**, *185*, 330 – 338.

(7) Scanlon, D. O.; Buckeridge, J.; Catlow, C. R. A.; Watson, G. W. Understanding doping

anomalies in degenerate p-type semiconductor LaCuOSe. *J. Mater. Chem. C* **2014**, *2*, 3429–3438.

(8) Alaria, J.; Borisov, P.; Dyer, M. S.; Manning, T. D.; Lepadatu, S.; Cain, M. G.; Mishina, E. D.; Sherstyuk, N. E.; Ilyin, N. A.; Hadermann, J.; Lederman, D.; Claridge, J. B.; Rosseinsky, M. J. Engineered spatial inversion symmetry breaking in an oxide heterostructure built from isosymmetric room-temperature magnetically ordered components. *Chem. Sci.* **2014**, *5*, 1599–1610.

(9) Pauling, L. The principles determining the structure of complex ionic crystals. *J. Am. Chem. Soc.* **1929**, *51*, 1010–1026.

(10) Born, M.; Huang, K. *Dynamical Theory of Crystal Lattices*; Clarendon Press, Oxford, 1954.

(11) Mott, N. F.; Littleton, M. J. Conduction in polar crystals. I. Electrolytic conduction in solid salts. *Trans. Faraday Soc.* **1938**, *34*, 485–499.

(12) Catlow, C. R. A.; Guo, Z. X.; Miskufova, M.; Shevlin, S. A.; Smith, A. G. H.; Sokol, A. A.; Walsh, A.; Wilson, D. J.; Woodley, S. M. Advances in computational studies of energy materials. *Phil. T. Roy. Soc. A* **2010**, *368*, 3379–3456.

(13) Torrance, J.; Metzger, R. Role of the Madelung energy in hole conductivity in copper oxides: Difference between semiconductors and high-T_c superconductors. *Phys. Rev. Lett.* **1989**, *63*, 1515.

(14) Fujishima, A.; Honda, K. Electrochemical Photolysis of Water at a Semiconductor Electrode. *Nature* **1972**, *238*, 37–38.

(15) Li, G.; Gray, K. A. The solid-solid interface: Explaining the high and unique photocatalytic reactivity of TiO_2-based nanocomposite materials. *Chem. Phys.* **2007**, *339*, 173 – 187.

(16) Scanlon, D. O.; Dunnill, C. W.; Buckeridge, J.; Shevlin, S. A.; Logsdail, A. J.; Wood-ley, S. M.; Catlow, C. R. A.; Powell, M. J.; Palgrave, R. G.; Parkin, I. P.; Watson, G. W.; Keal, T. W.; Sherwood, P.; Walsh, A.; Sokol, A. A. Band alignment of rutile and anatase TiO_2 from theory and experiment. *Nat. Mater.* **2013**, *12*, 798–801.

(17) Ihm, J.; Zunger, A.; Cohen, M. L. Momentum-space formalism for the total energy of solids. *J. Phys. C: Solid State Phys.* **1979**, *12*, 4409.

(18) Baur, W. H. Über die Verfeinerung der Kristallstrukturbestimmung einiger Vertreter des Rutiltyps: TiO_2, SnO_2, GeO_2 und MgF_2. *Acta Cryst.* **1956**, *9*, 515–520.

(19) Cromer, D. T.; Herrington, K. The Structures of Anatase and Rutile. *J. Am. Chem. Soc.* **1955**, *77*, 4708–4709.

(20) Baur, W. H. Atomabstände und Bindungswinkel im Brookit, TiO_2. *Acta Cryst.* **1961**, *14*, 214–216.

(21) Feist, T. P.; Davies, P. K. The soft chemical synthesis of TiO_2(B) from layered titanates. *J. Solid State Chem.* **1992**, *101*, 275 – 295.

(22) Filatov, S.; Bendeliani, N.; Albert, B.; Kopf, J.; Dyuzheva, T.; Lityagina, L. Crystalline structure of the TiO_2 II high-pressure phase at 293, 223, and 133 K according to single-crystal x-ray diffraction data. *Dok. Phys.* **2007**, *52*, 195–199.

(23) Swamy, V.; Dubrovinsky, L. S.; Dubrovinskaia, N. A.; Langenhorst, F.; Simionovici, A. S.; Drakopoulos, M.; Dmitriev, V.; Weber, H.-P. Size effects on the structure and phase transition behavior of baddeleyite TiO_2. *Solid State Commun.* **2005**, *134*, 541 – 546.

(24) Latroche, M.; Brohan, L.; Marchand, R.; Tournoux, M. New hollandite oxides: TiO_2(H) and $K_{0.06}TiO_2$. *J. Solid State Chem.* **1989**, *81*, 78 – 82.

(25) Akimoto, J.; Gotoh, Y.; Oosawa, Y.; Nonose, N.; Kumagai, T.; Aoki, K.; Takei, H. Topotactic Oxidation of Ramsdellite-Type $Li_{0.5}TiO_2$, a New Polymorph of Titanium Dioxide: TiO_2(R). *J. Solid State Chem.* **1994**, *113*, 27 – 36.

(26) Muscat, J.; Swamy, V.; Harrison, N. M. First-principles calculations of the phase stability of TiO_2. *Phys. Rev. B* **2002**, *65*, 224112.

(27) *Inorganic Crystal Structure Database*, http://www.fiz-karlsruhe.de/icsd_web.html

(28) De Angelis, F.; Di Valentin, C.; Fantacci, S.; Vittadini, A.; Selloni, A. Theoretical Studies on Anatase and Less Common TiO_2 Phases: Bulk, Surfaces, and Nanomaterials. *Chem. Rev.* **0**, *114*, 9708–9753.

(29) Trasatti, S. The absolute electrode potential: an explanatory note (Recommendations 1986). *J. Electroanal. Chem.* **1986**, *209*, 417–428.

(30) Jaeger, C. D.; Bard, A. J. Spin trapping and electron spin resonance detection of radical intermediates in the photodecomposition of water at titanium dioxide particulate systems. *J. Phys. Chem.* **1979**, *83*, 3146–3152.

(31) Ni, M.; Leung, M. K.; Leung, D. Y.; Sumathy, K. A review and recent developments in photocatalytic water-splitting using for hydrogen production. *Renew. Sust. Ener. Rev.* **2007**, *11*, 401 – 425.

(32) Kumar, S. G.; Devi, L. G. Review on Modified TiO_2 Photocatalysis under UV/Visible Light: Selected Results and Related Mechanisms on Interfacial Charge Carrier Transfer Dynamics. *J. Phys. Chem. A* **2011**, *115*, 13211–13241, PMID: 21919459.

(33) Amtout, A.; Leonelli, R. Optical properties of rutile near its fundamental band gap. *Phys. Rev. B* **1995**, *51*, 6842–6851.

(34) Kraeutler, B.; Bard, A. J. Heterogeneous photocatalytic decomposition of saturated

carboxylic acids on titanium dioxide powder. Decarboxylative route to alkanes. *J. Am. Chem. Soc.* **1978**, *100*, 5985–5992.

(35) Di Paola, A.; Bellardita, M.; Palmisano, L. Brookite, the Least Known TiO_2 Photocatalyst. *Catalysts* **2013**, *3*, 36–73.

(36) Catlow, C. R. A.; Mackrodt, W. C. *Computer Simulation of Solids*; Springer, Berlin, 1982.

(37) De Angelis, F.; Di Valentin, C.; Fantacci, S.; Vittadini, A.; Selloni, A. Theoretical Studies on Anatase and Less Common TiO_2 Phases: Bulk, Surfaces, and Nanomaterials. *Chem. Rev.* **2014**, *114*, 9708–9753.

(38) Egdell, R.; Eriksen, S.; Flavell, W. Oxygen deficient $SnO_2(110)$ and $TiO_2(110)$: A comparative study by photoemission. *Solid State Commun.* **1986**, *60*, 835–838.

(39) Murata, H.; Kataoka, Y.; Kawamoto, T.; Tanaka, I.; Taniguchi, T. Photocatalytic activity of α-PbO_2-type TiO_2. *Phys. Status Solidi-R* **2014**, *8*, 822–826.

(40) Pan, H.; Qiu, X.; Ivanov, I. N.; Meyer, H. M.; Wang, W.; Zhu, W.; Paranthaman, M. P.; Zhang, Z.; Eres, G.; Gu, B. Fabrication and characterization of brookite-rich, visible light-active TiO_2 films for water splitting. *Appl. Catal. B-Environ.* **2009**, *93*, 90 – 95.

(41) Yang, D.; Liu, H.; Zheng, Z.; Yuan, Y.; Zhao, J.-c.; Waclawik, E. R.; Ke, X.; Zhu, H. An Efficient Photocatalyst Structure: $TiO_2(B)$ Nanofibers with a Shell of Anatase Nanocrystals. *J. Am. Chem. Soc.* **2009**, *131*, 17885–17893, PMID: 19911792.

(42) Jiao, Y.; Chen, F.; Zhao, B.; Yang, H.; Zhang, J. Anatase grain loaded brookite nanoflower hybrid with superior photocatalytic activity for organic degradation. *Colloids Surf. A* **2012**, *402*, 66 – 71.

(43) Lee, H. U.; Lee, Y.-C.; Lee, S. C.; Park, S. Y.; Son, B.; Lee, J. W.; Lim, C.-H.; Choi, C.-J.; Choi, M.-H.; Lee, S. Y.; Oh, Y.-K.; Lee, J. Visible-light-responsive bicrys-

talline (anatase/brookite) nanoporous nitrogen-doped TiO_2 photocatalysts by plasma treatment. *Chem. Eng. J.* **2014**, *254*, 268 – 275.

(44) Zhu, S.-C.; Xie, S.-H.; Liu, Z.-P. Design and Observation of Biphase TiO_2 Crystal with Perfect Junction. *J. Phys. Chem. Lett.* **2014**, *5*, 3162–3168.

(45) Armstrong, A.; Armstrong, G.; Canales, J.; García, R.; Bruce, P. Lithium-Ion Intercalation into TiO_2-B Nanowires. *Adv. Mater.* **2005**, *17*, 862–865.

(46) Morgan, B. J.; Madden, P. A. Lithium intercalation into TiO_2(B): A comparison of LDA, GGA, and GGA+U density functional calculations. *Phys. Rev. B* **2012**, *86*, 035147.

(47) Melot, B. C.; Tarascon, J.-M. Design and Preparation of Materials for Advanced Electrochemical Storage. *Acc. Chem. Res.* **2013**, *46*, 1226–1238, PMID: 23282038.

(48) Subramanian, V.; Karki, A.; Gnanasekar, K.; Eddy, F. P.; Rambabu, B. Nanocrystalline TiO_2 (anatase) for Li-ion batteries. *J. Power Sources* **2006**, *159*, 186 – 192.

(49) Pfanzelt, M.; Kubiak, P.; Fleischhammer, M.; Wohlfahrt-Mehrens, M. TiO_2 rutile - An alternative anode material for safe lithium-ion batteries. *J. Power Sources* **2011**, *196*, 6815 – 6821.

(50) Zhang, S. B.; Wei, S. H.; Zunger, A. Intrinsic n-type versus p-type doping asymmetry and the defect physics of ZnO. *Phys. Rev. B* **2001**, *63*, 075205.

(51) Walsh, A.; Catlow, C. R. A.; Miskufova, M.; Sokol, A. A. Electron and hole stability in GaN and ZnO. *J. Phys.: Condens. Matter* **2011**, *23*, 334217.

(52) Walsh, A.; Buckeridge, J.; Catlow, C. R. A.; Jackson, A. J.; Keal, T. W.; Miskufova, M.; Sherwood, P.; Shevlin, S. A.; Watkins, M. B.; Woodley, S. M.; Sokol, A. A. Limits to Doping of Wide Band Gap Semiconductors. *Chem. Mater.* **2013**, *25*, 2924–2926.

(53) Bhachu, D. S.; Sathasivam, S.; Sankar, G.; Scanlon, D. O.; Cibin, G.; Carmalt, C. J.; Parkin, I. P.; Watson, G. W.; Bawaked, S. M.; Obaid, A. Y.; Al-Thabaiti, S.; Basahel, S. N. Solution Processing Route to Multifunctional Titania Thin Films: Highly Conductive and Photcatalytically Active Nb:TiO$_2$. *Adv. Funct. Mater.* **2014**, *24*, 5075–5085.

(54) Kafizas, A.; Noor, N.; Carmichael, P.; Scanlon, D. O.; Carmalt, C. J.; Parkin, I. P. Combinatorial Atmospheric Pressure Chemical Vapor Deposition of F:TiO$_2$; the Relationship between Photocatalysis and Transparent Conducting Oxide Properties. *Adv. Funct. Mater.* **2014**, *24*, 1758–1771.

(55) Orita, M.; Ohta, H.; Hirano, M.; Hosono, H. Deep-ultraviolet transparent conductive β-Ga$_2$O$_3$ thin films. *Appl. Phys. Lett.* **2000**, *77*, 4166–4168.

(56) Henrich, V. E.; Cox, P. A. *The surface science of metal oxides*; 1996.

(57) Linsebigler, A. L.; Lu, G.; Yates, J. T. Photocatalysis on TiO$_2$ Surfaces: Principles, Mechanisms, and Selected Results. *Chem. Rev.* **1995**, *95*, 735–758.

(58) Yang, H. G.; Sun, C. H.; Qiao, S. Z.; Zou, J.; Liu, G.; Smith, S. C.; Cheng, H. M.; Lu, G. Q. Anatase TiO$_2$ single crystals with a large percentage of reactive facets. *Nature* **2008**, *453*, 638–641.

(59) Lin, H.; Li, L.; Zhao, M.; Huang, X.; Chen, X.; Li, G.; Yu, R. Synthesis of High-Quality Brookite TiO$_2$ Single-Crystalline Nanosheets with Specific Facets Exposed: Tuning Catalysts from Inert to Highly Reactive. *J. Am. Chem. Soc.* **2012**, *134*, 8328–8331, PMID: 22559221.

(60) Yin, W.-J.; Tang, H.; Wei, S.-H.; Al-Jassim, M. M.; Turner, J.; Yan, Y. Band structure engineering of semiconductors for enhanced photoelectrochemical water splitting: The case of TiO$_2$. *Phys. Rev. B* **2010**, *82*, 045106.

(61) Deák, P.; Aradi, B.; Frauenheim, T. Quantitative theory of the oxygen vacancy and carrier self-trapping in bulk TiO_2. *Phys. Rev. B* **2012**, *86*, 195206.

(62) Deák, P.; Kullgren, J.; Frauenheim, T. Polarons and oxygen vacancies at the surface of anatase TiO_2. *Phys. Status Solidi-R* **2014**, *8*, 583–586.

(63) Luttrell, T.; Halpegamage, S.; Tao, J.; Kramer, A.; Sutter, E.; Batzill, M. Why is anatase a better photocatalyst than rutile? - Model studies on epitaxial TiO_2 films. *Sci. Rep.* **2014**, *4*, .

(64) *ChemShell, a Computational Chemistry Shell*, http://www.chemshell.org, 1999.

(65) Sherwood, P.; de Vries, A. H.; Guest, M. F.; Schreckenbach, G.; Catlow, C. R. A.; French, S. A.; Sokol, A. A.; Bromley, S. T.; Thiel, W.; Turner, A. J.; Billeter, S.; Terstegen, F.; Thiel, S.; Kendrick, J.; Rogers, S. C.; Casci, J.; Watson, M.; King, F.; Karlsen, E.; Sjøvoll, M.; Fahmi, A.; Schäfer, A.; Lennartz, C. QUASI: A general purpose implementation of the QM/MM approach and its application to problems in catalysis. *J. Mol. Struct. (Theochem.)* **2003**, *632*, 1–28.

(66) Dick, B. G.; Overhauser, A. W. Theory of the Dielectric Constants of Alkali Halide Crystals. *Phys. Rev.* **1958**, *112*, 90–103.

(67) Sokol, A. A.; Bromley, S. T.; French, S. A.; Catlow, C. R. A.; Sherwood, P. Hybrid QM/MM embedding approach for the treatment of localized surface states in ionic materials. *Int. J. Quantum Chem.* **2004**, *99*, 695–712.

(68) Sokol, A. A.; French, S. A.; Bromley, S. T.; Catlow, C. R. A.; van Dam, H. J. J.; Sherwood, P. Point defects in ZnO. *Faraday Discuss.* **2007**, *134*, 267–282.

(69) Dutta, G.; Sokol, A. A.; Catlow, C. R. A.; Keal, T. W.; Sherwood, P. Activation of Carbon Dioxide over Zinc Oxide by Localised Electrons. *ChemPhysChem* **2012**, *13*, 3453–3456.

(70) Buckeridge, J.; Bromley, S. T.; Walsh, A.; Woodley, S. M.; Catlow, C. R. A.; Sokol, A. A. One-dimensional embedded cluster approach to modeling CdS nanowires. *J. Chem. Phys.* **2013**, *139*, 124101.

(71) Butler, K. T.; Buckeridge, J.; Catlow, C. R. A.; Walsh, A. Crystal electron binding energy and surface work function control of tin dioxide. *Phys. Rev. B* **2014**, *89*, 115320.

(72) Buckeridge, J.; Catlow, C. R. A.; Scanlon, D. O.; Keal, T. W.; Sherwood, P.; Miskufova, M.; Walsh, A.; Woodley, S. M.; Sokol, A. A. Determination of the Nitrogen Vacancy as a Shallow Compensating Center in GaN Doped with Divalent Metals. *Phys. Rev. Lett.* **2015**, *114*, 016405.

(73) Guest, M. F.; Bush, I. J.; Van Dam, H. J. J.; Sherwood, P.; Thomas, J. M. H.; Van Lenthe, J. H.; Havenith, R. W. A.; Kendrick, J. The GAMESS-UK electronic structure package: algorithms, developments and applications. *Mol. Phys.* **2005**, *103*, 719–747.

(74) Bergner, A.; Dolg, M.; Küchle, W.; Stoll, H.; Preuß, H. Ab initio energy-adjusted pseudopotentials for elements of groups 13-17. *Mol. Phys.* **1993**, *80*, 1431–1441.

(75) Weigend, F.; Ahlrichs, R. Balanced basis sets of split valence, triple zeta valence and quadruple zeta valence quality for H to Rn: Design and assessment of accuracy. *Phys. Chem. Chem. Phys.* **2005**, *7*, 3297–3305.

(76) Zhao, Y.; Lynch, B. J.; Truhlar, D. G. Development and Assessment of a New Hybrid Density Functional Model for Thermochemical Kinetics. *J. Phys. Chem. A* **2004**, *108*, 2715–2719.

(77) Gale, J. D.; Rohl, A. L. The General Utility Lattice Program (GULP). *Mol. Simulat.* **2003**, *29*, 291–341.

(78) Born, M.; Huang, K. *Dynamical theory of crystal lattices*; Oxford University Press: Oxford, MA, USA, 1956.

(79) Krukau, A. V.; Vydrov, O. A.; Izmaylov, A. F.; Scuseria, G. E. Influence of the exchange screening parameter on the performance of screened hybrid functionals. *J. Chem. Phys.* **2006**, *125*, 224106.

(80) Kresse, G.; Hafner, J. *Ab initio* molecular dynamics for liquid metals. *Phys. Rev. B* **1993**, *47*, 558–561.

(81) Kresse, G.; Hafner, J. *Ab initio* molecular-dynamics simulation of the liquid-metal−amorphous-semiconductor transition in germanium. *Phys. Rev. B* **1994**, *49*, 14251–14269.

(82) Kresse, G.; Furthmüller, J. Efficiency of *ab-initio* total energy calculations for metals and semiconductors using a plane-wave basis set. *Comput. Mater. Sci.* **1996**, *6*, 15 – 50.

(83) Kresse, G.; Furthmüller, J. Efficient iterative schemes for *ab initio* total-energy calculations using a plane-wave basis set. *Phys. Rev. B* **1996**, *54*, 11169–11186.

(84) Blöchl, P. E. Projector augmented-wave method. *Phys. Rev. B* **1994**, *50*, 17953–17979.

Graphical TOC Entry
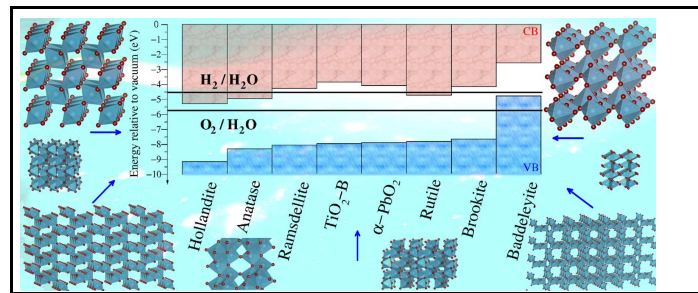
Small variation in local structure of TiO_2 polymorphs leads to a large variation in electronic properties.